ELSEVIER

Journal of Photochemistry and Photobiology A: Chemistry 120 (1999) 151–159

Journal of Photochemistry and Photobiology A:Chemistry

Kinetic investigation of electronic energy transfer processes following the pulsed dye-laser generation of excited atomic barium, Ba[6s6p($^1P_1$)], in the presence of atomic strontium

D. Husain[a,*], J. Lei[b], F. Castaño[c], M.N. Sánchez Rayo[c]

[a]*Department of Chemistry, University of Cambridge, Lensfield Road, Cambridge CB2 1EW, UK*
[b]*Department of Chemistry, King's College London, Strand, London WC2R 2LS, UK*
[c]*Departamento de Quimica Fisica, Universidad del Pais Vasco, Apartado 644, 48080, Bilbao, Spain*

Received 23 September 1998; accepted 20 October 1998

Abstract

The collisional behaviour of Ba[6s5d(^3D_J)], 1.151 eV above the $6s^2(^1S_0)$ electronic ground state, in the presence of atomic strontium, has been investigated in the 'long-time domain' (ca. 100 μs–1 ms) following the pulsed dye-laser excitation of barium vapour at elevated temperature at $\lambda = 553.5$ nm (Ba[6s6p($^1P_1$)] ← Ba[$6s^2(^1S_0)$]. Ba(^3D_J) is subsequently produced from the short-lived $^1P_1$ state ($\tau_e = 8.37 \pm 0.38$ ns) by a number of radiative and collisional processes. It may then be monitored in the 'long-time domain' by atomic spectroscopic marker methods involving either collisional activation of Ba(^3D_J) by Ba($^1S_0$) and He buffer gas to yield Ba[6s6p(^3P_J)] with subsequent emission from the $^3P_1$ state ($\tau_e = 1.2 \pm 0.1$ μs): Ba[6s6p($^3P_1$)] → Ba[$6s^2(^1S_0)$] + $h\nu$ ($\lambda = 791.1$ nm). Alternatively, emission from Ba($^1P_1$) may be monitored at long times following the generation of this short-lived state by energy pooling following self-annihilation of Ba(^3D_J) + Ba(^3D_J) from Ba[6s6p($^1P_1$)] → Ba[$6s^2(^1S_0)$] + $h\nu$ ($\lambda = 553.5$ nm). The generation of Ba(^3D_J) in the presence of atomic strontium yields emission in the long-time domain from Sr[5s5p($^3P_1$)] ($\tau_e = 19.6$ μs): Sr[5s5p($^3P_1$)] → Sr[$5s^2(^1S_0)$] + $h\nu$ ($\lambda = 689.3$ nm). Whilst the decay profiles at short times are complex in form, at long times all these atomic profiles show first-order kinetic removal with the decay coefficients for $\lambda = 791.1$ nm, 689.3 nm and 553.5 nm emissions in the ratio 1 : 2 : 2, consistent with overall third-order activation of the form: Ba(^3D_J) + Ba(^3D_J) + Sr($^1S_0$) → Sr(^3P_J) + 2Ba($^1S_0$). The mechanism is modelled in detail, including measurement of integrated emission intensities, yielding kinetic data for fundamental collisional processes. The overall rate constant for the third-order collisional activation of Sr[5s5p(^3P_J]) from 2Ba[6s5d(^3D_J)] + Sr[$5s^2(^1S_0)$] takes the upper limit of 5.8×10^{-27} cm^6 atom^{-2} s^{-1} ($T = 900$ K). The rate constant for the two body collisional quenching of Ba[6s5d(^3D_J)] by ground state atomic strontium, Sr[$5s^2(^1S_0)$], is found to be $(2.0 \pm 0.1) \times 10^{-12}$ cm^3 atom^{-1} s^{-1} ($T = 900$ K).

Keywords: Excited barium atoms; Ba(^{3}D); Laser excitation; Energy transfer to strontium atoms; Sr($^1S_0$); Sr(^{3}P) Collisional excitation; Rate processes

1. Introduction

Energy transfer processes between atomic states of different metallic species, especially those involving optically metastable states of alkaline-earth metal atoms, have been the objects of considerable attention in recent years [1–10]. This has arisen both for fundamental reasons and on account of the possibility of constructing high-power laser systems based on such processes [4,6,8,9]. The use of the time-domain for quantitative characterisation of processes in equilibrium-coupled systems involving Mg[3s3p(^3P_J)], Ca[4s4p(^3P_J)], Ca[4s3d($^1D_2$)] and Sr[5s5p(^3P_J)] has been described in detail by Husain and Roberts [2,4–6]. These authors have demonstrated the rapid establishment of equilibrium between Ca[4s4p(^3P_J)] and Sr[5s5p(^3P_J)] following the pulsed dye-laser excitation of calcium vapour at $\lambda = 657.3$ nm {Ca[4s4p($^3P_1$) ← $4s^2(^1S_0)$]} in the presence of strontium vapour, indicating coupling between Ca[4s4p-(^3P_J)] + Sr[$5s^2(^1S_0)$] and Sr[5s5p(^3P_J)] + Ca[$4s^2(^1S_0)$] via near-resonant electronic exchange processes. Similarly, rapid electronic energy equilibrium between Ca[4s3d($^1D_2$)] and Mg[3s3p(^3P_J)] was demonstrated following pulsed laser excitation of mixtures of calcium and magnesium vapours either at $\lambda = 457.1$ nm {Mg[3s3p($^3P_1$)] ← Mg[$3s^2(^1S_0)$]} or at $\lambda = 457.5$ nm {Ca[4s3d($^1D_2$)] ← Ca[$4s^2(^1S_0)$]} via the near- resonant electronic energy exchange processes coupling Ca[4s3d($^1D_2$)] + Mg[$3s^2(^1S_0)$] and Mg[3s3p(^3P_J)] + Ca[$4s^2(^1S_0)$]. The equilibria were demonstrated by the equality in the measured first-order decay coefficients for removal of these excited atoms under a wide range of

*Corresponding author. Tel.: +44-01223-336 463.

1010-6030/99/$ – see front matter
PII: S1010-6030(98)00428-6

conditions including the presence of helium buffer gas and also gases which quench the excited states with high collisional efficiency.

Benard and co-workers have observed that electronic energy transfer takes place from Mg[3s3p(^3P_J)] to Ca[4s^2($^1S_0$)] in a flow-discharge system [10] and that energy transfer from Ca[4s4p(^3P_J)] to Sr{5s^2($^1S_0$)] takes place following optical generation of Ca[4s4p(^3P_J)] in a mixture of Ca and Sr atoms [3]. These authors have also reported the observation of electronic energy transfer processes from Mg[3s3p(^3P_J)] to yield Ca[4s4d($^1D_2$)] and excited Bi atoms [8] following laser generation of Mg[3s3p($^3P_1$) at $\lambda = 457.1$ nm following rapid equilibration within the ^3P_J spin-orbit manifold of atomic magnesium. Energy transfer from Mg[3s3p(^3P_J)] to atomic Sm has been studied by Stanfill et al. [9] following laser generation of Mg[3s3p($^3P_1$)] in a Mg/Sm mixed system and report a rate constant for this electronic energy transfer process of $k = (1.6 \pm 0.5) \times 10^{-9}$ cm^3 atoms^{-1} s^{-1}. Kallenbach et al. [1] have reported the study of energy transfer from atomic barium to strontium following the initial laser generation of Ba[6s6p($^1P_1$)] at $\lambda = 553.5$ nm {Ba[6s6p($^1P_1$)] ← Ba-[6s^2($^1S_0$)] in strontium–barium vapour mixtures. The cross sections for the collisional population of the D and P levels in Sr from Ba[6s6p($^1P_1$)] have been estimated to be about 1.5 and 3 $\times 10^{-19}$ m^2, respectively, though no further details about these processes have yet been published to the best of our knowledge.

In the present paper, measurements have been attempted to observe energy transfer from Sr[5s5p(^3P_J)] to atomic barium following laser excitation of Sr[5s5p($^3P_1$)] at $\lambda = 689.3$ nm {Sr[5s5p($^3P_1$)] ← Sr[5s^2($^1S_0$)]} in Sr–Ba mixed vapours at $\lambda = 689.3$. No emission was observed from electronically excited barium atoms and hence one can conclude that the energy transfer process via the exothermic routes initially yielding Ba[6s5d(^3D_J)] and Ba[6s5d($^1D_2$)] are too inefficient to be observed in this system. On the other hand, we have observed emission from Sr[5s5p($^3P_1$)] in the time-resolved mode following the pulsed dye-laser excitation of Ba/Sr mixed vapour at the barium resonance line $\lambda = 553.5$ nm. We describe the investigation of collisional energy transfer processes from Ba[6s5d(^3D_J)] to yield Sr[5s5p(^3P_J)] by monitoring the atomic emissions from Ba[6s6p($^1P_1$)], Ba[6s6p($^3P_1$)] and Sr[5s5p($^3P_1$)] in the time-domain. Quantitative characterisation of these time profiles coupled with their comparison under a range of experimental conditions and measurement of integrated emission intensities, suitably calibrated for optical response, are employed for determining a mechanism for the main transfer processes and for quantifying appropriate fundamental collisional rate data.

2. Experimental

The experimental arrangement for the study of time-resolved atomic emission from Ba[6s6p($^1P_1$)], Ba[6s6p($^3P_1$)] and Sr[5s5p($^3P_1$)] essentially follows that described in previous papers employed to study kinetic processes in barium vapours with noble gases and reactions of Ba[6s5d(^3D_J)] with methyl halides [11–16]. Ba[6s5d(^3D_J)] may be generated by the combination of radiative and collisional transfer processes following the initial pulsed dye-laser excitation of atomic barium via the allowed transition at $\lambda = 553.5$ nm {Ba[6s6p($^1P_1$)] ← Ba[6s^2($^1S_0$)]} at a elevated temperature ($T > 900$ K) [14–16]. Ba[6s6p($^1P_1$)] was thus produced using the second harmonic (532 nm) of a Nd:YAG primary laser (10 Hz) (J.K. Lasers, System 2000) to pump a dye-laser (Rhodamine chloride 590, typically 1.0 $\times 10^{-4}$ M in methanol, Exciton) operating at $\lambda = 553.55$ nm. The population of the low lying Ba[6s5d(^3D_J)] atoms then was monitored using the time-resolved spectroscopic markers at $\lambda =$ 791.1 nm {Ba[6s6p($^3P_1$)] → Ba[6s^2($^1S_0$)]} following collisional excitation of Ba(^3D_J) by Ba and He atoms, and at $\lambda = 553.5$ nm {Ba[6s6p($^1P_1$)] → Ba[6s^2($^1S_0$)]} from energy pooling emission arising from self-annihilation of two Ba[6s5d(^3D_J)] atoms. The population of Sr[5s5p(^3P_J)] was measured directly by time-resolved atomic emission from Sr($^3P_1$) at $\lambda = 689.3$ nm {Sr[5s5p($^3P_1$)] → Sr[5s^2($^1S_0$)]}. These three atomic emissions are monitored as a function of temperature, that is, as functions of [Ba] and [Sr].

Two monochromator–photomultiplier detection systems were employed as in various previous measurements. (A) The first involved a photomultiplier tube with an S20 response (E.M.I., 9797B) whose gain (G) can sensibly be fitted to the form ln G (G in arb. units) = 8.7 ln V (V in volts)−54.4 [14,15]. This was combined with a small high throughput 'Minichrom' monochromator (MC1-02-10288, Fastie–Ebert mounting; f/4; focal length 74 mm, range 200–800 nm). The wavelength response of the photomultiplier–grating combination (pm–grating) was calibrated against a quartz-halogen lamp which had previously been calibrated against a spectral radiometer (International Light Inc., USA, IL783). (B) The second monochromator–photomultiplier system employed an infra-red sensitive photomultiplier tube (Hamamatsu R632-S1 response). This is a 12-dynode device with a photocathode material of Ag–O–Cs and a sensitivity range of ca. 400–1200 nm. The gain (G) of the tube can sensibly be described by the form ln(G) = 8.48 ln V (V in volts)−47.28 ($\gamma = 0.998$) from the commercial gain characteristic. This was combined with a further high throughput compact monochromator (Speirs Robertson GM 100; aperture ratio $f = 4.7$; fixed slits 0.5 mm) that included a grating with optical sensitivity at long wavelength (Speirs Robertson GM 100–5; range 350–1100 nm; 590 grooves/mm; blaze 500 nm). The wavelength response of this pm–grating combination was again calibrated using a quartz halogen lamp and the above spectral radiometer. The combination of the wavelength response of the p.m.–grating systems and the gain characteristics of the p.m. tubes with voltage are employed in determining integrated atomic intensities from decay profiles on a common intensity scale. The forms of the decay profiles themselves are, of course,

independent of these calibrations. The population of $Sr[5s5p(^3P_J)]$ was measured directly time-resolved atomic emission at $\lambda = 689.3$ nm. The emissions at $\lambda = 553.5$ nm and 689.3 nm were measured with detector system A; that at $\lambda = 791.1$ nm employed system B. A mixture of chips of Ba and Sr was prepared to yield a mixture of the vapours of these two atomic gases at elevated temperatures. These three atomic emissions are monitored as a function of temperature, that is, as functions of [Ba] and [Sr]. One should note that, for the purpose of kinetic analysis, the atomic concentration of Sr is typically higher than that of Ba at a given temperature on the basis of vapour pressure data for pure barium or strontium vapours. All materials (Ba, Sr and He) were prepared as described in previous publications.

3. Results and discussion

Following pulsed dye-laser excitation of a mixture of Ba and Sr vapours in the presence of excess helium buffer gas at the barium resonance wavelength at $\lambda = 553.5$ nm $\{Ba[6s6p(^1P_1)] \leftarrow Ba[6s^2(^1S_0)]\}$, strong atomic emission from both electronically excited barium and strontium was observed. Figs. 1 and 2 show examples of the digitised output indicating the exponential decay profiles of the time-resolved barium atomic emissions from the energy transfer excited marker state at $\lambda = 791.1$ nm from $Ba(^3P_1)$, and from the energy pooled state at $\lambda = 553.5$ nm from $Ba(^1P_1)$ following the laser excitation at 553.5 nm in the temperature region from 860 to 1000 K. In this temperature range, [Ba] varies from 2.3×10^{13} cm^{-3} to 5.1×10^{14} cm^{-3}, and [Sr] from 4.9×10^{14} to 8.8×10^{15} cm^{-3}

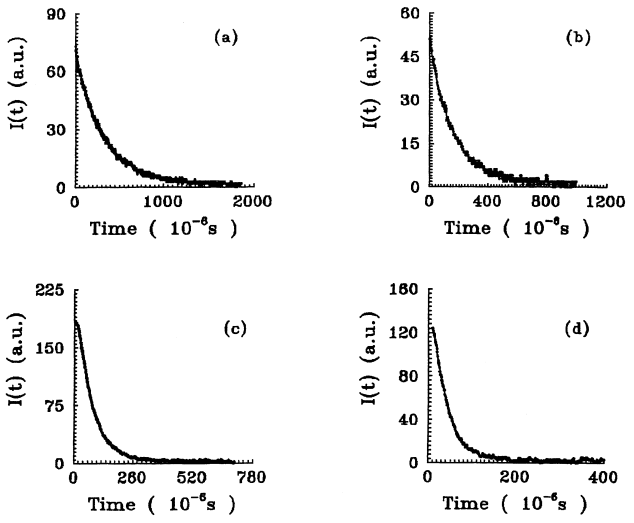

Fig. 1. Examples of the digitised output of the time-resolved emission in the long-time domain from atomic barium at $\lambda = 791.1$ nm $Ba[6s6p(^3P_1)] \rightarrow Ba[6s^2(^1S_0)]$ following the pulsed dye-laser excitation of atomic barium at $\lambda = 553.5$ nm $\{Ba[6s6p(^1P_1)] \leftarrow Ba[6s^2(^1S_0)]\}$ in the presence of strontium vapour and excess helium buffer gas ($p_{He} = 80$ Torr) at various temperatures. T (K): (a) 880 (b) 920 (c) 960 (d) 1000.

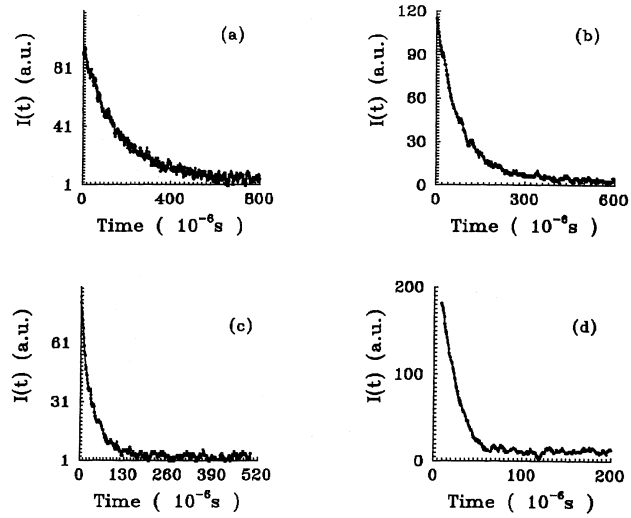

Fig. 2. Examples of the digitised output of the time-resolved emission in the long-time domain from atomic barium at $\lambda = 553.5$ nm $\{Ba[6s6p(^1P_1)] \rightarrow Ba[6s^2(^1S_0)]\}$ following the pulsed dye-laser excitation of atomic barium at the resonance wavelength $\{Ba[6s6p(^1P_1)] \leftarrow Ba[6s^2(^1S_0)]\}$ in the presence of strontium vapour and excess helium buffer gas ($p_{He} = 80$ Torr) at various temperatures. T (K): (a) 880 (b) 920 (c) 960 (d) 1000.

[17]. We may immediately note the long-time domain of these emissions in the context of the short radiative lifetimes of these excited states of Ba, $\tau_e(6^1P_1) = 8.37 \pm 0.38$ ns, $\tau_e(^3P_1) = 1.2\,\mu$s, and of $Sr(^3P_1)$ (19.6 μs). The associated computerised first-order profiles constructed from Figs. 1 and 2 are shown in Figs. 3 and 4, respectively. Examples indicating the decays of the time-resolved atomic

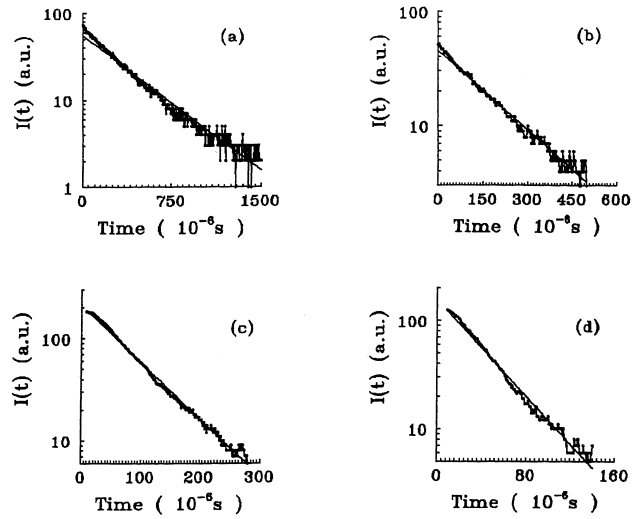

Fig. 3. Examples of the first-order decay profiles constructed from the digitised output of the time-resolved emission in the long-time domain from atomic barium at $\lambda = 791.1$ nm $Ba[6s6p(^3P_1)] \rightarrow Ba[6s^2(^1S_0)]$ following the pulsed dye-laser excitation of atomic barium at $\lambda = 553.5$ nm $\{Ba[6s6p(^1P_1)] \leftarrow Ba[6s^2(^1S_0)]\}$ in the presence of strontium vapour and excess helium buffer gas ($p_{He} = 80$ Torr) at various temperatures. T (K): (a) 880 (b) 920 (c) 960 (d) 1000.

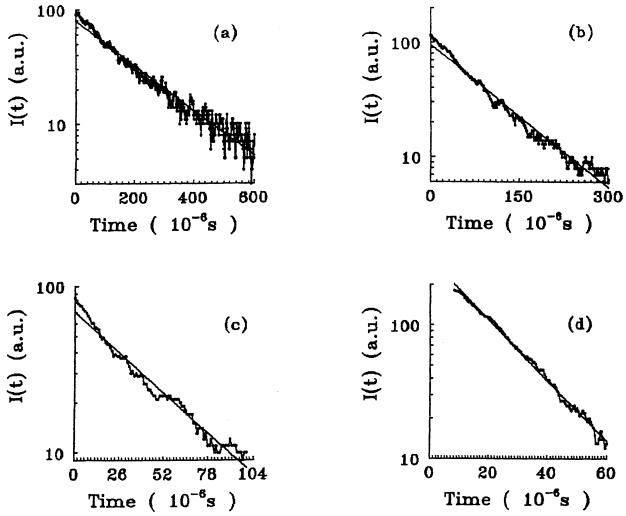

Fig. 4. Examples of the first-order decay profiles constructed from the digitised output of the time-resolved emission in the long-time domain from atomic barium at $\lambda = 553.5$ nm $\{Ba[6s6p(^1P_1)] \rightarrow Ba[6s^2(^1S_0)]\}$ following the pulsed dye-laser excitation of atomic barium at the resonance wavelength $\{Ba[6s6p(^1P_1)] \leftarrow Ba[6s^2(^1S_0)]\}$ in the presence of strontium vapour and excess helium buffer gas ($p_{He} = 80$ Torr) at various temperatures. T (K): (a) 880 (b) 920 (c) 960 (d) 1000.

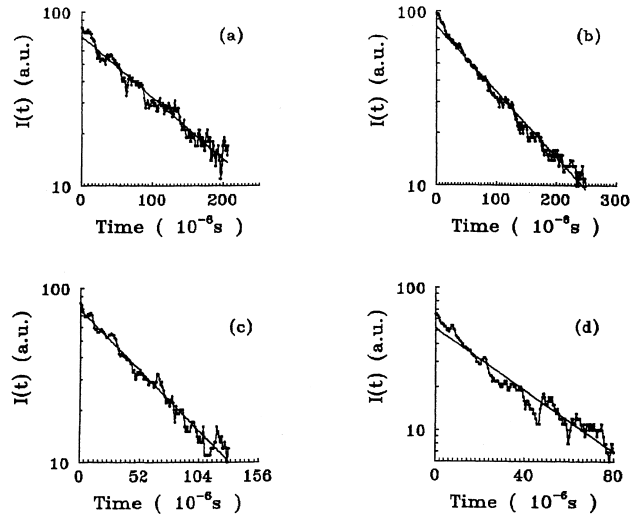

Fig. 6. Examples of the first-order decay profiles constructed from the digitised output of the time-resolved emission in the long-time domain from atomic strontium at $\lambda = 689.3$ nm $\{Sr[5s5p(^3P_1)] \rightarrow Sr[5s^2(^1S_0)]\}$ following the pulsed dye-laser excitation of atomic barium at $\lambda = 553.5$ nm $\{Ba[6s6p(^1P_1)] \leftarrow Ba[6s^2(^1S_0)]\}$ in the presence of strontium vapour and excess helium buffer gas ($p_{He} = 80$ Torr) at various temperatures. T (K): (a) 880 (b) 920 (c) 960 (d) 1000.

emissions at $\lambda = 689.3$ nm from $Sr(^3P_1)$ for the same experimental conditions as in Figs. 1 and 2 are given in Fig. 5. Fig. 6 shows the first-order decay profiles constructed from the digitised outputs of Fig. 5. All the three atomic decay profiles display good first-order behaviour and the corresponding decay coefficients can be derived from the linear fittings of these first-order plots.

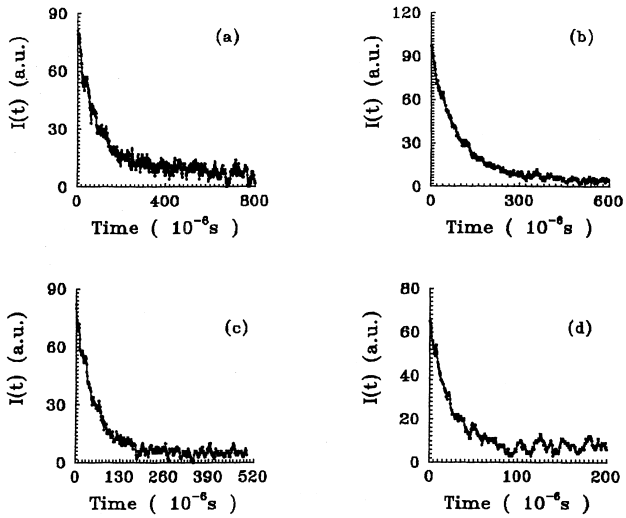

Fig. 5. Examples of the digitised output of the time-resolved emission in the long-time domain from atomic strontium at $\lambda = 689.3$ nm $\{Sr[5s5p(^3P_1)] \rightarrow Sr[5s^2(^1S_0)]\}$ following the pulsed dye-laser excitation of atomic barium at $\lambda = 553.5$ nm $\{Ba[6s6p(^1P_1)] \leftarrow Ba[6s^2(^1S_0)]\}$ in the presence of strontium vapour and excess helium buffer gas ($p_{He} = 80$ Torr) at various temperatures. T (K): (a) 880 (b) 920 (c) 960 (d) 1000.

The increase of the decay coefficients with temperature reflects the increasing role of collisional quenching of the long-lived, excitation transfer precursor, $Ba[6s5d(^3D_J)]$, by ground state atomic barium and strontium. The variations of decay coefficients for the three atomic emissions with temperature are shown in Fig. 7. The decay coefficients of excited strontium at $\lambda = 689.3$ nm are similar to those of excited barium at $\lambda = 553.5$ nm in the lower temperature region (ca. 840–930 K). These become marginally smaller at higher temperature on account of the effects of radiation trapping of the strontium 689.3 nm emission and the colli-

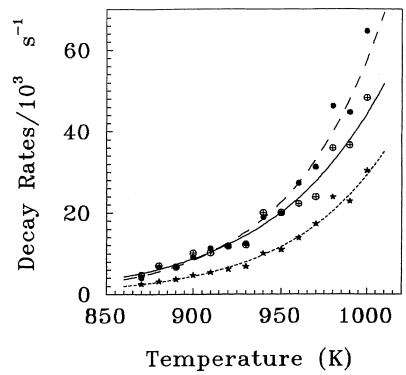

Fig. 7. Variation of the first-order decay coefficients (k') for the time-resolved atomic emission from atomic barium and strontium in the long-time domain $\{\lambda = 791.1$ nm $Ba[6s6p(^3P_1)] \rightarrow Ba[6s^2(^1S_0)]$; $\lambda = 553.5$ nm $\{Ba[6s6p(^1P_1)] \rightarrow Ba[6s^2(^1S_0)]\}$; $\lambda = 689.3$ nm $Sr[5s5p(^3P_1)] \rightarrow Sr[5s^2(^1S_0)]\}$ following the pulsed dye-laser excitation of atomic barium at $\lambda = 553.5$ nm $\{Ba[6s6p(^1P_1)] \leftarrow Ba[6s^2(^1S_0)]\}$ in the presence of strontium vapour and excess helium buffer gas ($p_{He} = 80$ Torr) at various temperatures. * k' (791.1 nm); ● k' (553.5 nm); ⊕ k' (689.3 nm).

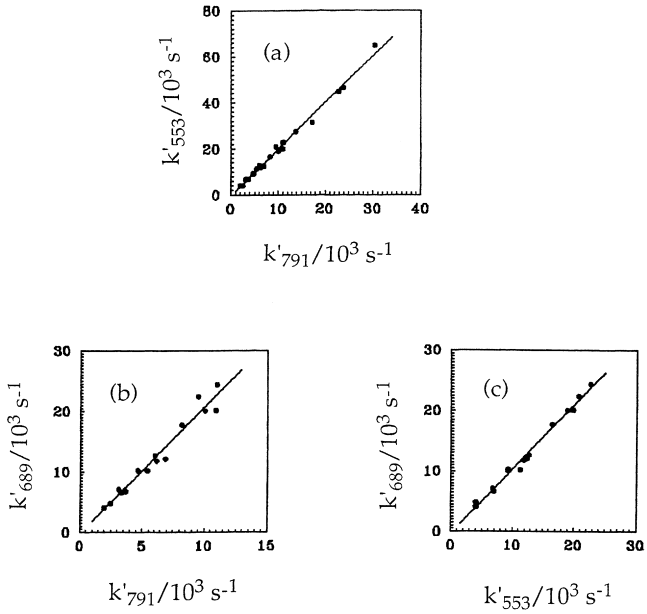

Fig. 8. Comparison of the first-order decay coefficients (k') for the time-resolved atomic emission from atomic barium and strontium in the long-time domain {$\lambda = 791.1$ nm, Ba[6s6p($^3P_1$)] → Ba[6s^2($^1S_0$)]; $\lambda = 553.5$ nm, Ba[6s6p($^1P_1$)] → Ba[6s^2($^1S_0$)]; $\lambda = 689.3$ nm Sr[5s5p($^3P_1$)] → Sr[5s^2($^1S_0$)]} following the pulsed dye-laser excitation of atomic barium at $\lambda = 553.5$ nm, {Ba[6s6p($^1P_1$)] ← Ba[6s^2($^1S_0$)]} in the presence of strontium vapour and excess helium buffer gas ($p_{He} = 80$ Torr) in the temperature range 840–920 K; The slopes are (a) $k'_{553.5}/k'_{791.1} = 2.02$; (b) $k'_{689.3}/k'_{791.1} = 2.09$;$k'_{689.3}/k'_{553.5} = 1.06$.

sional quenching of Ba(^3D_J) at high barium and strontium concentrations on these two emission profiles but these do not influence the collisional transfer processes (vide infra). Nevertheless, the first-order decay coefficients of the Sr($^3P_1$) emission can be compared with that from Ba($^1P_1$) and from Ba($^3P_1$) in the lower temperature region. These results are displayed in Fig. 8, together with a comparison of the decay coefficients of the atomic barium emissions at $\lambda = 553.5$ and 791.1 nm. The comparisons of the decay coefficients for atomic emissions from Sr($^3P_1$) at $\lambda = 689.3$ nm, from Ba($^1P_1$) at $\lambda = 553.5$ nm and from Ba($^3P_1$) at $\lambda = 791.1$ nm are essentially in the ratio of 2 : 2 : 1 within experimental error (±5%) ($k'_{553}/k'_{791} = 2.02$; $k'_{689}/k'_{791} = 2.09$; $k'_{689}/k'_{553} = 1.06$ where k' are the measured first-order decay coefficients. This indicates, given the established mechanism of the two spectroscopic markers for Ba(^3D_J), that the collisional transfer involves two Ba(^3D_J) atoms in the overall production of Sr(^3P_J) in this region of high strontium atomic density.

3.1. Kinetic processes and rate equations

From the above measurements, one can conclude that Sr[5s5p(^3P_J)] results from an overall three-body mechanism involving two Ba[6s5d(^3D_J)] atoms and one and ground state Sr[5s^2($^1S_0$)] following the laser excitation of a mixture of Ba–Sr vapour at $\lambda = 553.5$ nm in the presence of excess He buffer gas. Thus, in the case of high strontium atomic density, this can be written kinetically as

$$2\mathrm{Ba}[6s5d(^3D_J)] + \mathrm{Sr}[5s^2(^1S_0)] \xrightarrow{k_{3BS}} \mathrm{Sr}[5s5p(^3P_J)] + 2\mathrm{Ba}[6s^2(^1S_0)] \quad (1)$$

The contribution from an overall endothermic two-body collisional transfer process

$$\mathrm{Ba}[6s5d(^3D_J)] + \mathrm{Sr}[5s^2(^1S_0)] \xrightarrow{k_{2BS}} \mathrm{Sr}[5s5p(^3P_J)] + \mathrm{Ba}[6s^2(^1S_0)] \quad (2)$$

should be included initially, although its efficiency is low on energetic grounds. The overall mechanism can be simply presented by Fig. 9.

The rate equations to describe the variation of [Ba(^3D_J)] and [Sr(^3P_J)] in the 'long-time domain' following Eqs. (1) and (2) for the collisional processes also including spontaneous emission can hence be formally written as:

$$\frac{d[\mathrm{Ba}(^3D_J)]}{dt} = -\gamma_{Ba}[\mathrm{Ba}(^3D_J)] - \frac{k_{3BS}[\mathrm{Ba}(^3D_J)]^2[\mathrm{Sr}]}{2} \quad (3)$$

$$\frac{d[\mathrm{Sr}(^3P_J)}{dt} = k_{3BS}[\mathrm{Ba}(^3D_J)]^2[\mathrm{Sr}]/2 + k_{2BS}[\mathrm{Ba}(^3D_J)][\mathrm{Sr}] - \gamma_{Sr}[\mathrm{Sr}(^3P_J)] \quad (4)$$

The rate equations for describing the time evolution of the energy transfer excited state marker, Ba[6s6p(^3P_J)], and the energy pooled marker state, Ba[6s6p($^1P_1$)], from the long-

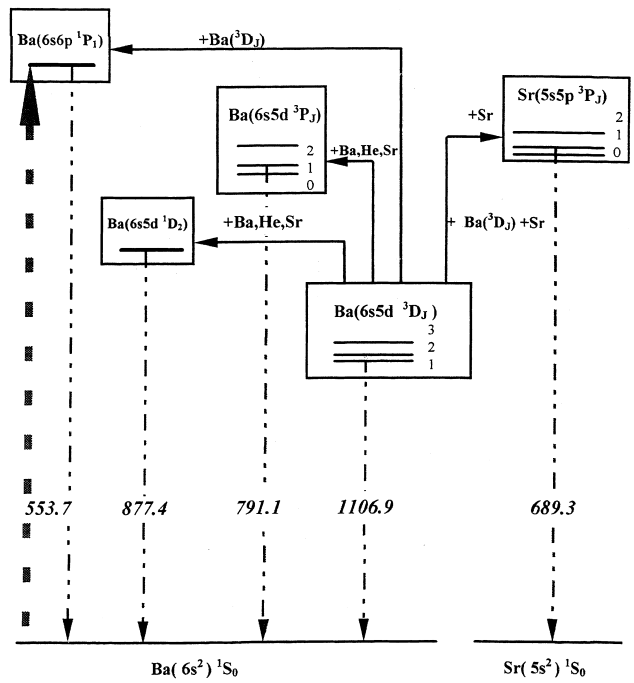

Fig. 9. Schematic diagram of the kinetic processes taking place following the pulsed dye-laser excitation of atomic barium at $\lambda = 553.5$ nm {Ba[6s6p($^1P_1$)] ← Ba[6s^2($^1S_0$)]}, in the presence of strontium vapour and excess helium buffer gas at elevated temperature.

lived precursor state Ba[6s5d(^{3}D$_J$)], are given in references [14–16] and described mechanistically in the experimental section. The effective overall decay coefficients (γ) for Ba[6s5d(^{3}D$_J$)] and Sr[5s5p(^{3}P$_J$)] can be written as follows:

$$\gamma_{Ba} = \frac{g_{Ba}A_{Ba,nm}}{F_{Ba}} + \frac{\beta_{Ba}}{p_{He}} + k_{Ba,qHe}[He] + k_{Ba,qBa}[Ba] + k_{Ba,qSr}[Sr] \quad (5)$$

$$\gamma_{Sr} = \frac{g_{Sr}A_{Sr,nm}}{F_{Sr}} + \frac{\beta_{Sr}}{p_{He}} + k_{Sr,qHe}[He] + K_{Sr,qBa}[Ba] + k_{Sr,qSr}[Sr] \quad (6)$$

This notation appears complex but simply takes account of the differing rate constants for energy transfer (k), coefficients for spontaneous emission (A_{nm}), radiation trapping (g), equilibrium constants connecting specific spin–orbit states (F), collisional quenching constants (k_q) and diffusional loss (β) for specific atomic states involved here and is clear on inspection in any given case. Hence, here the states Ba[6s5d(^{3}D$_J$)] and Sr[5s5p(^{3}P$_J$)] are labelled by Ba and Sr. Thus, for example, the term $k_{Ba,qSr}$[Sr] represents the collisional quenching of Ba[6s5d(^{3}D$_J$)] by strontium atoms which involves the two-body collision transfer process to the Sr[5s5p(^{3}P$_J$)] state. With the exception of the term $k_{Sr,qBa}$[Ba] representing collisional quenching of Sr[5s5p(^{3}P$_J$)] by ground state atomic barium, the rate constant for which is unknown, the other terms in Eq. (6), e.g., g_{Sr}, $A_{Sr,\,nm}$, β_{Sr}, $k_{Sr,qHe}$ and $k_{Sr,qsr}$ can be found in references [18–25]. Hence the effective lifetime of Sr[5s5p(^{3}P$_J$)], $1/\gamma_{Sr}$, can be calculated to be of the order of 10 μs at a temperature $T = 850$ K.

For the present experimental conditions, it is always the case that [Ba^{3}D] ≪ [Ba] and [Sr^{3}P] ≪ [Sr]. Suppose the overall three-body collisional transfer constitutes only a small part of the removal of Ba[6s5d(^{3}D$_J$)], i.e., $k_{3BS}[^3D_J]^2[Sr]/2 \ll \gamma_{Ba}[^3D_J]$ and, at time $t = 0$, [Sr^{3}P$_J$] = 0 0 and Ba[^{3}D$_J$] = $N_{Ba,0}$, we may obtain the solution for the rate equation Eq. (3):

$$[Ba(^3D_J)] = N_{Ba,0}\ \exp(-\gamma_{Ba}\ t) \quad (7)$$

On this basis, the decay profiles of Ba[6s5d(^{3}D$_J$)] are characterised by single exponential forms. It can be obtained from the solution of the rate Eq. (4) that the decay profiles of Sr[5s5p(^{3}P$_J$)], generated by the overall three-body and two-body collisional mechanisms from Ba[6s5d(^{3}D$_J$)], are determined by three exponential parameters: γ_{Ba}, $2\gamma_{Ba}$ and γ_{Sr}. The experimental observation demonstrated that the contribution from the two-body collisional mechanism for excitation of Sr(^{3}P$_J$) is negligible and hence the appropriate terms can be neglected. At lower temperatures in the region of $T < 900$ K, the decay of Sr[5s5p(^{3}P$_J$)] is dominated by the radiative decay of Sr($^3P_1$) which is characterised by a radiative lifetime of 19.6 μs, modified by the function F_{Sr} describing the equilibrium connection between the states in the ^{3}P$_J$ spin-orbit manifold. Further, the decay of Ba[6s5d(^{3}D$_J$)] dominated by the collisional quenching Ba(^{1}S$_0$) [14,15] and Sr(^{1}S$_0$) (vide infra) with effective lifetimes of the order of hundreds of microseconds. Hence, it can be concluded that $\gamma_{Sr} \gg \gamma_{Ba}$ and the solution for Sr(^{3}P$_J$) can be simply written as:

$$[Sr(^3P_J)] = \left\{\frac{k_{3BS}[Sr](N_{Ba,0})^2}{2(\gamma_{Sr} - 2\gamma_{Ba})}\right\}\exp(-2\gamma_{Ba}\ t) \quad (8)$$

Thus the decay rate of Sr[5s5p(^{3}P$_J$)] emission ($\lambda = 689.3$ nm) = $2\gamma_{Ba}$ as is that of the of energy pooling emission from Ba[6s6p(^{1}P$_1$)] ($\lambda = 553.5$ nm) and double that of the spectroscopic marker for Ba(^{3}D$_J$) at $\lambda = 791.1$ nm due to energy transfer excitation to Ba[6s6p(^{3}P$_1$)] for lower temperatures, i.e., lower atomic densities of Ba and Sr. Alternatively, the emission at $\lambda = 689.3$ nm reflects the rate of production of Sr[5s5p(^{3}P$_J$)] from two Ba(^{3}D$_J$) atoms in the presence of Sr(^{1}S$_0$). This is consistent with the experimental observations shown in Fig. 9. However, at higher temperatures, emission from Sr[5s5p(^{3}P$_1$)] at $\lambda = 689.3$ nm is subject to significant radiation trapping [18] causing a reduction in its decay rate. Of course, the collisional quenching of Ba[6s5d(^{3}D$_J$)] by the higher densities of Ba and Sr atoms will cause this metastable state to decay more rapidly. Eventually, the decay rate of Ba[6s5d(^{3}D$_J$)] will become larger than that of Sr[5s5p(^{3}P$_J$)], i.e., $\gamma_{Sr} < \gamma_{Ba}$. For example, at $T = 970$ K, $(1/\gamma_{Sr}) \sim 250$ μs and $(1/\gamma_{Ba}) \sim 60$ μs. In this case, the decay the emission at $\lambda = 689.3$ nm will be dominated by the decay coefficient, γ_{Sr}. This will become smaller than that for the energy pooling emission at $\lambda = 553.5$ nm, consistent with the experimental observation (Fig. 7).

The rate constant for the collisional quenching of Ba[6s5d(^{3}D$_J$)] by Sr(^{1}S$_0$) strontium atoms can be derived from the decay profiles of the atomic marker emissions for Ba(^{3}D$_J$) at $\lambda = 791.1$ nm (γ_{791}) and $\lambda = 553.5$ nm (γ_{553}). For a fixed pressure of helium buffer gas, following Eq. (5), we have [14–16]:

$$\gamma_{791} - k_{Ba,qBa}[Ba] = C + k_{Ba,qSr}[Sr] \quad (9)$$

$$\gamma_{553} - 2k_{Ba,qBa}[Ba] = 2\{C + k_{Ba,qSr}[Sr]\}$$

where C is a constant. Thus, a plot of $\{\gamma_{791} - k_{Ba,qBa}[Ba]\}$ or $\{\gamma_{553} - 2k_{Ba,qBa}[Ba]\}/2$ against the concentration of atomic strontium yields the rate constant for the collisional quenching Ba(^{3}D$_J$) by ground state strontium atoms, $k_{Ba,qSr}$[Sr]. The constant $k_{Ba,qBa}$ has been reported earlier work for this temperature regime [14–16], namely, $k_{Ba,qBa} = 2.4 \times 10^{-11}$ cm^3 atom^{-1} s^{-1}.

Fig. 10 shows the variation of $\{\gamma_{791} - k_{Ba,qBa}[Ba]\}$ and $\{\gamma_{553} - 2k_{Ba,qBa}[Ba]\}$ against density of atomic strontium, [Sr]. For the former (791.1 nm), this yields $k_{Ba,qSr} = 1.98 \times 10^{-12}$ cm^3 atom^{-1} s^{-1} and for the latter (553.5 nm), this yields $k_{Ba,qSr} = 2.05 \times 10^{-12}$ cm^3 atom^{-1} s^{-1} for the temperature range employed here. Hence we conclude that the rate constant for the collisional quenching of Ba[6s5d(^{3}D$_J$)] by Sr(^{1}S$_0$) is characterised by $k_{Ba,qSr} = (2.0 \pm 0.1) \times$

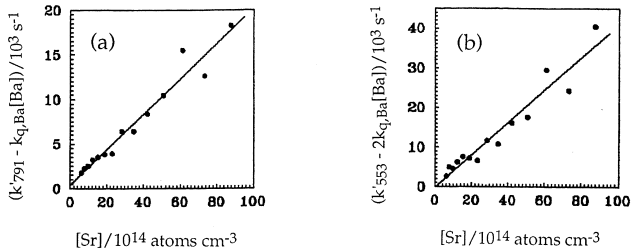

Fig. 10. Variations of (a) $\{k'_{791} - k_{q,Ba}[Ba]\}$ and (b) $\{k'_{553} - 2k_{q,Ba}[Ba]\}$ as a function of the concentration of atomic strontium following the pulsed dye-laser excitation of atomic barium at $\lambda = 553.5$ nm $\{Ba[6s6p(^1P_1] \leftarrow Ba[6s^2(^1S_0)]\}$ in the presence of strontium vapour and excess helium buffer gas ($p_{He} = 80$ Torr) at elevated temperatures.

10^{12} cm^3 atom^{-1} s^{-1}, constituting the first measurement of this quantity to the best of our knowledge. This can be compared with analogous measurement of Malins and Benard [26] describing the collision quenching Ca[4s4p(^{3}P$_J$)] by Mg[3s^2(^{1}S$_0$)] characterised by $k_{qMg} = 9.0 \times 10^{-13}$ cm^3 atom^{-1} s^{-1}. It must be emphasised that the above measurement of $k_{Ba,qSr}$ was based on the calculated vapour pressure data using reference [17] for the pure elements, Ba or Sr, at equilibrium at a given temperature. Although these will be close to those of a Ba–Sr mixed vapour in a static system, the real values of the Ba and Sr atomic densities in the mixed Ba–Sr vapour are difficult to characterise [4,5] accurately. Hence, the true error in the above value is difficult to quantify and the reported accuracy of the value of $k_{Ba,qSr}$ may be considered with some caution.

The integrated intensity of emission from atomic strontium at $\lambda = 689.3$ nm may be calculated following the solution of the rate Eq. (4):

$$I_{Sr,689} = \left(\frac{g_{Sr}\ A_{Sr,nm}}{F_{Sr}}\right) \int [Sr(^3P_J)]\, dt = \left(\frac{g_{Sr}\ A_{Sr,nm}}{F_{Sr}}\right) \frac{k_{3BS}[Sr][N_{Ba,0}]^2}{4} + \frac{k_{2BS}[Sr](N_{Ba,0})}{\gamma_{Sr}\gamma_{Ba}} \quad (11)$$

As indicated earlier, in the present measurements, overall two body collisional activation of Sr[5s5p(^{3}P$_J$)] may be neglected. Hence the integrated intensity of the emission from Sr[5s5p(^{3}P$_J$)] at $\lambda = 689.3$ nm is directly proportional to the atomic density of Sr(^{3}P$_J$) and to [Ba^{3}D$_J$]^2. Fig. 11 shows the temperature variations of the integrated intensities of the emission from atomic barium at $\lambda = 791.1$ nm and $\lambda = 553.5$ nm, and from atomic strontium at $\lambda = 689.3$ nm derived from the decay profiles suitably calibrated for optical response. They all decrease with increasing temperature, i.e., with increasing [Ba(^{1}S$_0$)] and [Sr(^{1}S$_0$)], thus arising mainly from the collisional quenching of Ba[6s5d(^{3}D$_J$)] by atomic barium and strontium. The similar variations of the integrated intensities of $I_{Ba,553}$ and $I_{Sr,689}$ are shown in Fig. 11, differing from that of $I_{Ba,791}$, and reflecting the activation in the long-time regime of

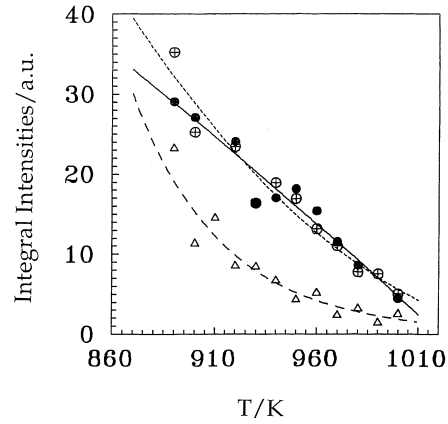

Fig. 11. Temperature variation of the integrated atomic emission intensities ($I_{791,553,689}$) at $\lambda = 791.1$ nm [Ba(^{3}P$_1$ – ^{1}S$_0$)], $\lambda = 553.5$ nm [Ba(^{1}P$_1$ –^{1} S$_0$)] and $\lambda = 689.3$ nm [Sr(^{3}P$_1$ –^{1} S$_0$)] following the pulsed dye-laser excitation of atomic barium at $\lambda = 553.5$ nm $\{Ba[6s6p(^1P_1)] \leftarrow Ba[6s^2(^1S_0)]\}$ in the presence of strontium vapour and excess helium buffer gas ($p_{He} = 80$ Torr) at elevated temperatures. Δ I_{791}; $\oplus$ I_{553}; ● I_{689}

[Ba6s6p(^{1}P$_1$)] and Sr[5s5p(^{3}P$_J$)] by two Ba[6s5d(^{3}D$_J$)] atoms.

If we suppose that the three body collision dominates the production of Sr[5s5p(^{3}P$_J$)] and that the emission $\lambda = 553.5$ nm dominates the decay of [Ba6s6p(^{1}P$_1$)], the integrated intensities $I_{Ba,553}$ and $I_{Sr,689}$ are related as follows:

$$\frac{I_{Sr,689}}{I_{Ba,553}} = \left(\frac{g_{Sr}\ A_{Sr,nm}}{F_{Sr}\gamma_{Sr}}\right)\left(\frac{k_{3BS}}{k_{Ep}}\right)[Sr] = C_{Sr}\left(\frac{k_{3BS}}{k_{Ep}}\right)[Sr] \quad (12)$$

$$\frac{I_{Sr,689}}{I_{Ba,553}C_{Sr}} = \left(\frac{k_{3BS}}{k_{Ep}}\right)[Sr] \quad (13)$$

where k_{Ep} is the rate constant for energy pooling between two [Ba^{3}D$_J$] atoms to yield Ba^{1}P$_1$. $C_{Sr} = g_{Sr}A_{Sr,nm}/F_{Sr}\gamma_{Sr}$ is a parameter concerned with the decay of Sr[5s5p(^{3}P$_J$)], monitored by the emission at $\lambda = 689.3$ nm, and whose decay coefficient is determined by spontaneous emission, diffusion, collisional quenching, radiation trapping and the intermultiplet equilibrium conditions within Sr(^{3}P$_J$), and which can be calculated overall from the appropriate rate constants [18–25]. Eqs. (12) and (13) indicate that this ratio, $I_{Sr,689}/I_{Ba,553}$, should be in direct proportion to the concentration of atomic strontium. The experimentally measured variation for this ratio is shown in Fig. 12. This plot emphasises the dominant role of overall three body collisional activation of Sr[5s5p(^{3}P$_J$)] following laser excitation of the Ba/Sr mixture at $\lambda = 553.5$ nm. At the same time, the slope of this linear plot yields the value of k_{3BS}/k_{Ep}. The value of k_{Ep} for the rate constant for the energy pooling between two Ba[6s5d(^{3}D$_J$)] atoms has been reported by Gallagher et al. [27] to be given by $k_{Ep} \geq 8.1 \times 10^{-12}$ cm^3 atom^{-1} s^{-1} ($T = 860$ K). This, in turn, yields an upper limit for the three body rate constant for the overall process described in Eq. (1) to yield Sr[5s5p(^{3}P$_J$)] from 2Ba[6s5d(^{3}D$_J$)] and ground state atomic strontium as $k_{3BS} \leq 5.83 \times 10^{-27}$ cm^6 atom^{-2} s^{-1}. Again, it should be stressed here as hitherto that

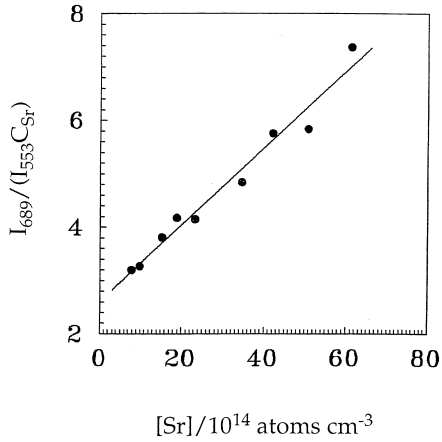

Fig. 12. Variation of the function I_{689} /($I_{553}C_{Sr}$) as a function of the concentration of atomic strontium following the pulsed dye-laser excitation of atomic barium at $\lambda = 553.5$ nm {Ba[6s6p($^1P_1$)] ← Ba[6s^2-($^1S_0$)]} in the presence of strontium vapour and excess helium buffer gas ($p_{He} = 80$ Torr) at elevated temperatures.

the atomic density of strontium was calculated for the pure metal following reference [17].

In broad conclusion, the present measurements have demonstrated that, in contrast to electronic energy transfer processes for excited states of other alkaline earth metal atoms, where transfer processes proceeded by two body collisions amongst different metal atoms [2–11,26], the principal transfer process involved here overall is three body in nature, involving two Ba[6s5d(^3D_J)] atoms and Sr[5s^2($^1S_0$)]. Two body transfer between Ba[6s5d(^3D_J)] atoms and Sr[5s^2($^1S_0$)] to yield Sr[5s5p(^3P_J)] is relatively small and the resulting emission is weak, only observed at low density of atomic strontium. Process (2) is, indeed endothermic ($\Delta H = 5292$ cm^{-1}), where the energy defect from translation at these temperatures can only be provided by ca. 1 in 5000 collisions. The energy defect for the three-body process (2) ($\Delta H = -3990$ cm^{-1}) is taken up by translational energy in the separated atoms.

A standard combination of two-body processes may be proposed in this case for the overall three body excitation mechanism involving a dimer of Ba_2^* formed from the collision of two Ba[6s5d(^3D_J)] atoms, analogous to the dimer of Mg_2^* involved in energy pooling between two Mg[3s3p(^3P_J)] [28], and finally stabilised by Sr($^1S_0$), namely,

$$Ba[6s5d(^3D_J)] + Ba[6s5d(^3D_J)] \underset{k_{-1}}{\overset{k_1}{\rightleftarrows}} Ba_2^* \quad (14)$$

$$Ba_2^* + Sr[5s^2(^1S_0)] \xrightarrow{k_2} 2Ba[6s^2(^1S_0)] + Sr[5s5p(^3P_J)] \quad (15)$$

In the standard third-order limit when $k_{-1} \gg k_2$[Sr], then $k_{3BS} = 2k_1k_2/k_{-1}$. In the strong collision approximation, k_1 and k_2 may be estimated as collision frequencies using hard-sphere models [29–31] yielding $k_1 \approx 2.6 \times 10^{-10}$ cm^3 atoms^{-1} s^{-1} and $k_2 \approx 6.1 \times 10^{-10}$ cm^3 atoms^{-1} s^{-1}. Hence, from the measured value of $k_{3BS} \leq 5.83\ 10^{-27}$ cm^6 atoms^{-2} s^{-1} above, this yields $\tau(Ba_2^*) = 1/k_{-1} \approx 2 \times 10^{-8}$ s.

An alternative standard mechanism may be suggested involving the dimer BaSr*:

$$Ba[6s5d(^3D_J)] + Sr[5s^2(^1S_0)] \underset{k_{-1}}{\overset{k_1}{\rightleftarrows}} BaSr^* \quad (16)$$

$$BaSr^* + Ba[6s5d(^3D_J)] \xrightarrow{k_2} 2Ba[6s^2(^1S_0)] + Sr[5s5p(^3P_J)] \quad (17)$$

The absorption spectra of the analogous dimers, CaMg, SrMg and SrCa, have been reported by Miller et al. [32]. A similar argument to that above for the interpretation of the measured overall three body rate constant using the strong collision approximation with this mechanism yields $\tau(BaSr^*) \approx 2 \times 10^{-8}$ s.

Acknowledgements

We thank the Cambridge Overseas Scholarship Trustees for a Research Studentship held by J.L. during the tenure of this work. J.L. also thanks the O.R.S. for an award. We also thank the E.P.S.R.C. of Great Britain for the initial purchase of the laser system. Finally, we are also indebted to Dr. George Jones of DERA (Fort Halstead) for encouragement and helpful discussions.

References

[1] A. Kallenbach, M. Gunther, R. Kunnemeyer, M. Koch, J. Phys. B: At. Mol. Phys. 19 (1986) 2645.
[2] D. Husain, G. Roberts, J. Chem. Soc., Faraday Trans. 2, 81 (1985) 101.
[3] R.J. Malins, A.D. Logan, D.J. Benard, Chem. Phys. Lett. 83 (1981) 605.
[4] D. Husain, G. Roberts, J. Chem. Soc., Faraday Trans. 2, 84 (1988) 1213.
[5] D. Husain, G. Roberts, J. Chem. Soc., Faraday Trans. 2, 81 (1985) 87.
[6] D. Husain, G. Roberts, J. Phys. Chem. 92 (1988) 2079.
[7] A.T. Pritt, D. Patel, D.J. Benard, J. Phys. Chem. 90 (1986) 72.
[8] M.A. Chowdhury, D.J. Benard, J. Phys. Chem. 91 (1987) 2086.
[9] J.D. Stanfill, R.S.F. Chang, N. Djeu, Chem. Phys. Lett. 142 (1987) 275.
[10] D.J. Benard, P.J. Love, W.D. Slafer, Chem. Phys. Lett. 48 (1977) 321.
[11] D. Husain, Lei Jie, F. Castaño, M.N.S. Rayo, J. Photochem. Photobiol. A: Chem. 107 (1997) 1.
[12] D. Husain, Lei Jie, F. Castaño, M.N.S. Rayo, Anales de Quimica 93 (1997) 125.
[13] D. Husain, Lei Jie, F. Castaño, M.N.S. Rayo, Laser Chem. 17 (1997) 53.
[14] S. Antrobus, D. Husain, Lei Jie, J. Photochem. Photobiol. A: Chem. 103 (1997) 1.
[15] S. Antrobus, D. Husain, Lei Jie, J.Photochem. Photobiol., A: Chem. 103 (1997) 11.
[16] S. Antrobus, D. Husain, Lei Jie, Anales de Quimica 92 (1996) 17.
[17] C.B. Alcock, V.P. Itkin, M.K. Horrigan, Can. Metallurgical Quarterly 23 (1994) 309.
[18] D. Husain, Lei Jie, J. Photochem. Photobiol., A: Chem. 87 (1995) 89.

[19] D. Husain, G. Roberts, Chem. Phys. 127 (1988) 203.
[20] D. Husain, J. Schifino, J. Chem. Soc., Faraday Trans. 2, 80 (1984) 321.
[21] D. Husain, G. Roberts, J. Chem. Soc., Faraday Trans. 2, 81 (1985) 1085.
[22] M.D. Havey, L.C. Balling, J.J. Wright, Phys. Rev. A 13 (1976) 1269.
[23] J.F. Kelly, M. Harris, A. Gallagher, Phys. Rev. A 37 (1988) 2354.
[24] E.N. Borisov, N.P. Penkin, T.P. Redko, Opt. Spectrosc. 59 (1985) 426.
[25] S.R. Langhoff, C.W. Bauschlicher Jr., H. Partridge, Int. J. Quantum Chem. 18 (1984) 457.
[26] R.J. Malins, D.J. Benard, Chem. Phys. Lett. 74 (1980) 321.
[27] J.A. Neuman, A.C. Gallagher, J. Cooper, Phys. Rev. A 50 (1994) 1292.
[28] D. Husain, G. Roberts, J. Chem. Soc., Faraday Trans. II 82 (1986) 21.
[29] I.W.M. Smith, Kinetics and dynamics of elementary gas reactions, Butterworths, London, 1980, pp. 173–243.
[30] V.N. Kondratiev, E.E. Nikitin, Gas-phase reactions, Springer, Berlin, 1981, pp. 96–124.
[31] P.W. Atkins, Physical Chemistry, 5th ed., Oxford University Press, 1994, pp. 861–959.
[32] J.C. Miller, B.S. Ault, L. Andrews, J. Chem. Phys. 67 (1977) 2478.